crystals

MDPI

Article

Two-Dimensional Lattices with Lanthanoids, Anilato Ligands and Formamide

Samia Benmansour *, Antonio Hernández-Paredes, Kilian Defez-Aznar and Carlos J. Gómez-García *

Departamento de Química Inorgánica, Universidad de Valencia, C/Dr. Moliner 50, 46100 Burjasot, Valencia, Spain; antonio.hernandez-paredes@uv.es (A.H.-P.); kideaz@alumni.uv.es (K.D.-A.)
* Correspondence: sam.ben@uv.es (S.B.); carlos.gomez@uv.es (C.J.G.-G.)

Abstract: Here, we illustrate the use of formamide (fma) and anilato-type ligands to build two-dimensional lattices with lanthanoids. Thus, we describe the synthesis and crystal structure of four lattices formulated as $[Ln_2(C_6O_4X_2)_3(fma)_6]\cdot 6fma$ with Ln/X = La/Cl (**1**), La/Br (**2**), Eu/Cl (**3**), and Eu/Br (**4**), where $C_6O_4X_2^{2-}$ = dianion of 3,6-disubstituted-2,5-dihydroxy-1,4-benzoquinone with X = Cl (chloranilato) and X = Br (bromanilato). Single crystal X-ray analysis shows that the four compounds crystallize in the triclinic *P*-1 space group and present two-dimensional, very distorted hexagonal lattices with the lanthanoids ions in the vertex coordinated by three anilato ligands forming the sides of the distorted hexagons that appear as rectangles. The rectangles are disposed parallel to their long sides in a brick wall fashion. The nona-coordination of the lanthanoids is completed by three formamide molecules. These layered compounds include three additional formamide molecules per lanthanoid atom, located in the interlayer space inside the channels formed by the eclipsed packing of the layers. We discuss the differences observed among these compounds due to the change of the lanthanoid ion (La and Eu) and of the substituent group X in the anilato ligand (Cl and Br).

Keywords: lanthanoids; chloranilato; bromanilato; 2D honeycomb lattices; formamide; X-ray crystal structures; 6,3-topology

Citation: Benmansour, S.; Hernández-Paredes, A.; Defez-Aznar, K.; Gómez-García, C.J. Two-Dimensional Lattices with Lanthanoids, Anilato Ligands and Formamide. *Crystals* **2023**, *13*, 939. https://doi.org/10.3390/cryst13060939

Academic Editors: Helmut Cölfen and Jesús Sanmartín-Matalobos

Received: 28 April 2023
Revised: 23 May 2023
Accepted: 7 June 2023
Published: 11 June 2023

1. Introduction

According to IUPAC [1], MOFs can be defined as coordination networks formed by organic ligands containing potential voids. These porous coordination networks have experienced a huge interest in the 21st century, resulting in the synthesis of several thousands of MOFs with large porosities and surface areas, including examples with flexible skeletons and chemically functionalized cavities [2]. Of course, the control and modulation of the pore sizes and shapes, in order to modulate the properties of the MOFs, constitutes one of the most challenging tasks in the synthesis of these materials [3,4].

Although most MOFs contain transition metal atoms, there is an increasing interest in the synthesis of lanthanoid-based metal–organic frameworks (Ln-MOFs). This interest is based on the many properties and potential applications that they show. Thus, besides the well-known applications of many MOFs, such as gas storage and separation [5], catalysis [6], magnetic, optical, and chemical sensing [7–9], water absorption [10], etc., Ln-MOFs present additional properties, such as magnetism, including single-molecule and single-ion magnets (SMM and SIM), that makes them potential candidates for other applications in spintronics and quantum information processing [11] or as luminescent-based chemical sensors [12].

Besides three-dimensional (3D) MOFs, the synthesis of two-dimensional (2D) MOFs has gained a lot of attention in the last years, most likely due to the discovery of graphene and other 2D layered materials. These efforts have yielded several 2D MOFs with interesting properties and applications [13,14].

Many different ligands have been used to construct these MOFs. Some of them are from the family of 3,6-disubstituted-2,5-dihydroxy-1,4-benzoquinone dianions = $C_6O_4X_2^{2-}$, known as anilato ligands (Scheme 1a). These ligands present interesting advantages as they show different coordination modes such as: bidentate terminal (*1k*^{2}*O,O′*, Scheme 1b), bis-bidentate (*1k*^{2}*O,O′;2k*^{2}*O″,O‴*, Scheme 1c), monodentate (*1kO*), monodentate-bidentate (*1kO;2k*^{2}*O′,O″*), and even more complex modes (*1k*^{2}*O,O′;2k*^{2}*O″,O‴;3kO″*) [15]. The bidentate and bis-bidentate coordination modes are the most common ones and, as observed for the topologically equivalent oxalate ligand, result in the same type of structures from mononuclear tris(anilato)metalate complexes [16,17] to polymeric 1D, 2D, and 3D lattices, although with larger cavities and channels [15,18–22].

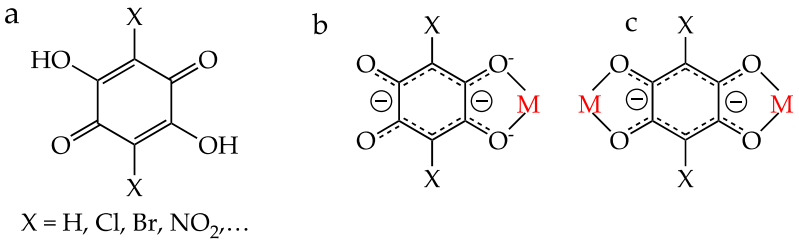

Scheme 1. (**a**) Anilato-type ligands and main coordination modes: (**b**) terminal bidentate and (**c**) bridging bis-bidentate.

Anilato-based MOFs with lanthanoids constitute a growing family since the very first reports of Raymond et al. [23], and, especially, Robson and Abrahams et al. [24,25]. A recent review by some of us [22] showed that there are more than 140 known compounds prepared with anilato ligands ($C_6O_4X_2^{2-}$ with X = H, F, Cl, Br, Cl/CN, CH_3, NO_2, and t-Bu) with all the lanthanoids ions (except Pm) and different solvents acting as co-ligands, such as H_2O [24,25], dimethyl sulfoxide [26,27], dimethylformamide [28,29], dimethylacetamide [30], ethanol [23], ethylene glycol [31], etc. Surprisingly, formamide has been used only in one case [32] among the more than 140 anilato–lanthanoid compounds reported to date [22].

The several families of compounds prepared with different solvents, lanthanoids, and anilato ligands [22] have clearly demonstrated that the final topology and structure depend on several factors: (i) the size of the Ln^{III} ion, (ii) the X groups of the anilato ligands, (iii) the shape and size of the coordinated solvent molecules, (iv) the synthetic method, and even (v) post synthetic solvent exchange treatment [33].

As there is only one reported example with formamide as solvent: $[Er_2(C_6O_4Cl_2)_3(fma)_6]\cdot 4fma\cdot 2H_2O$ [32], we have explored the possibility of preparing other lattices with this solvent and different lanthanoid metal ions using chloranilato and bromanilato (X = Cl and Br, Scheme 1). These attempts have led to the synthesis of four isostructural compounds formulated as $[Ln_2(C_6O_4X_2)_3(fma)_6]\cdot 6fma$ with Ln/X = La/Cl (**1**), La/Br (**2**), Eu/Cl (**3**), and Eu/Br (**4**). Here, we show the synthesis and structure of the four compounds and a detailed study of the differences observed in these four compounds caused by the change in X and in the lanthanoid ion.

2. Materials and Methods

Chloranilic acid, bromanilic acid, $La(NO_3)_3\cdot 6H_2O$, $Eu(NO_3)_3\cdot 6H_2O$, and fma are all commercial and were used as received without any further purification. All the compounds were obtained as single crystals using a layering method described below.

Synthesis of $[La_2(C_6O_4Cl_2)_3(fma)_6]\cdot 6fma$ (1) Single crystals of compound **1** were obtained by carefully layering, at room temperature, a solution of chloranilic acid, $H_2C_6O_4Cl_2$ (6.2 mg, 0.03 mmol) in 6.7 mL of methanol on top of a solution of $La(NO_3)_3.6H_2O$ (8.7 mg, 0.02 mmol) in 4.5 mL of fma. The tube (300 mm length and 5 mm diameter) was sealed and allowed to stand for one week to obtain purple prismatic single crystals suitable for X-ray

diffraction that were freshly picked and covered with paratone oil (to avoid solvent loss) to be characterized by single crystal X-ray diffraction.

Synthesis of $[La_2(C_6O_4Br_2)_3(fma)_6]\cdot 6fma$ (2) Purple prismatic single crystals of compound **2** were obtained in the same way as **1**, but using bromanilic acid, $H_2C_6O_4Br_2$ (6.0 mg, 0.02 mmol) in 4.5 mL of methanol, instead of chloranilic acid.

Synthesis of $[Eu_2(C_6O_4Cl_2)_3(fma)_6]\cdot 6fma$ (3) Purple prismatic single crystals of compound **3** were obtained in the same way as **1**, but using $Eu(NO_3)_3.6H_2O$ (8.9 mg, 0.02 mmol) instead of $La(NO_3)_3\cdot 6H_2O$.

Synthesis of $[Eu_2(C_6O_4Cl_2)_3(fma)_6]\cdot 6fma$ (4) Purple prismatic single crystals of compound **4** were obtained in the same way as **2**, but using $Eu(NO_3)_3.6H_2O$ (8.9 mg, 0.02 mmol) instead of $La(NO_3)_3\cdot 6H_2O$.

IR spectroscopy. IR spectra were performed on KBr pellets with a Bruker Equinox 55 spectrometer in the wavelength range 400–4000 cm^{-1}.

X-ray crystallography. Single crystals of all compounds were mounted on glass fibres with a viscous hydrocarbon oil to coat the crystals. The crystals were immediately transferred to a cold N_2 stream for data collection. X-ray data were collected on a Supernova diffractometer equipped with a graphite monochromated Enhance (Mo) X-ray Source (λ = 0.71073 Å) at 120 K. The program CrysAlisPro, Oxford Diffraction Ltd., was used for unit cell determinations and data reduction [34]. Empirical absorption correction was performed using spherical harmonics, implemented in the SCALE3 ABSPACK scaling algorithm. All compounds crystallize in the triclinic *P*-1 space group. Crystal structures were solved by direct methods with the SIR92 program [35] and refined against all F^2 values with the SHELXL-2014 program [36], using the WinGX2014.1 graphical user interface [37]. Non-hydrogen atoms were refined anisotropically, and hydrogen atoms were assigned fixed isotropic displacement parameters. Hydrogen atom positions were calculated geometrically and refined using the riding model. For the four compounds, hydrogen atoms of the ligands were set in calculated positions and refined as riding atoms, whereas the H atoms of crystallized formamide molecules, in some cases, could not be found nor calculated. For compound **2**, the use of some bond lengths restraints, applied on atoms belonging to formamide solvent molecules, has been reasonably imposed like DFIX and ISOR. In compound **3**, the use of some bond lengths restraints, applied on atoms belonging to dynamic moieties, has been reasonably imposed like RIGU and ISOR. Regarding compound **4**, the use of some bond lengths restraints, applied on atoms belonging to formamide solvent, has been reasonably imposed like ISOR and DFIX.

Complete tables with bond distances for compounds **1**–**4** are provided in the Supplementary Materials. A summary of the data collection and structure refinement for compounds **1**–**4** is given in Tables 1 and 2. Crystallographic data for the structures reported in this paper have been deposited in the Cambridge Crystallographic Data Centre with CCDC numbers 2259696–2259699. These data can be downloaded via www.ccdc.cam.ac.uk/deposit@ccdc.cam.ac.uk (accessed on 1 April 2023).

Table 1. Crystal data and structure refinement parameters for compounds $[La_2(C_6O_4X_2)_3(fma)_6]\cdot 6fma$ with X = Cl(**1**) and Br(**2**).

Compound	$[La_2(C_6O_4Cl_2)_3(fma)_6]\cdot 6fma$	$[La_2(C_6O_4Br_2)_3(fma)_6]\cdot 6fma$
Ref	**1**	**2**
CCDC	2259696	2259697
Empirical formula	$C_{15}H_5Cl_3LaN_6O_{12}$	$C_{15}H_8Br_3LaN_6O_{12}$
Formula weight	706.51	842.91
Crystal system	triclinic	triclinic
Space group	*P*-1	*P*-1

Table 1. *Cont.*

a (Å)	8.9314(10)	8.9686(9)
b (Å)	10.5972(9)	10.7072(12)
c (Å)	14.5498(13)	14.5975(11)
α (°)	75.639(7)	75.178(8)
β (°)	84.309(8)	83.957(7)
γ (°)	76.755(8)	76.664(9)
Volume (Å^3)	1297.3(2)	1317.0(2)
Z	2	2
Density (calculated) (g/cm^3)	1.809	2.126
Absorption coefficient (mm^{-1})	2.022	6.239
F(000)	682	796
Crystal size (mm^3)	0.07 × 0.04 × 0.02	0.07 × 0.04 × 0.02
2θ range for data (°)	3.372–25.048	3.367–25.036
Reflections collected	15226	8761
Data	4582	4651
Restraints	0	51
Parameters	343	352
Goodness-of-fit on F^2	1.062	1.052
R_1 [I > 2s(I)]	0.0488	0.0452
wR_2 (all data)	0.1228	0.0954
Largest diff. peak/hole/e Å^{-3}	1.126 and −0.897	1.278 and −0.954

Table 2. Crystal data and structure refinement parameters for compounds $[Eu_2(C_6O_4X_2)_3(fma)_6]\cdot 6fma$ with X = Cl (**3**) and Br (**4**).

Compound	$[Eu_2(C_6O_4Cl_2)_3(fma)_6]\cdot 6fma$	$[Eu_2(C_6O_4Br_2)_3(fma)_6]\cdot 6fma$
Ref	**3**	**4**
CCDC	2259698	2259699
Empirical formula	$C_{15}H_5Cl_3EuN_6O_{12}$	$C_{15}H_8Br_3EuN_6O_{12}$
Formula weight	729.64	861.00
Crystal system	triclinic	triclinic
Space group	*P*-1	*P*-1
a (Å)	8.8487(4)	8.8978(6)
b (Å)	10.5840(5)	10.6669(7)
c (Å)	14.2341(6)	14.3447(10)
α (°)	75.534(4)	75.168(6)
β (°)	84.718(4)	84.539(5)
γ (°)	76.350(4)	76.145(6)
Volume (Å^3)	1253.59(10)	1276.99(16)
Z	2	2
Density (calculated) (g/cm^3)	1.933	2.239

Table 2. *Cont.*

Absorption coefficient (mm^{-1})	2.891	7.218
F(000)	714	818
Crystal size (mm^3)	0.11 × 0.08 × 0.04	0.09 × 0.05 × 0.02
2θ range for data (°)	3.309–25.048	6.75–50.1
Reflections collected	4432	8637
Data	4008	4496
Restraints	42	74
Parameters	343	334
Goodness-of-fit on F^2	1.047	1.032
R_1 [I > 2s(I)]	0.0296	0.0496
wR_2 (all data)	0.0662	0.1223
Largest diff. peak/hole/e $Å^{-3}$	1.495 and −0.956	2.15 and −2.55

3. Results

3.1. Synthesis and IR Spectra

The synthesis of compounds **1–4** was performed following the same layering method but using different $Ln(NO_3)_3 \cdot nH_2O$ with chloranilic and bromanilic acids, and fma and methanol as solvents. As expected, since amides have a larger affinity towards lanthanoids than methanol [38], the resulting structures contain Ln^{III} ions coordinated to formamide rather than to methanol. The IR spectra of the four compounds are very similar, as expected, given their isostructurality and close composition. They show the expected bands associated with the anilato ligands and fma molecules. The main differences are observed in the C-X bands (X = Cl and Br) of the anilato ligands (see supporting information).

3.2. Crystal Structure of $[Ln_2(C_6O_4X_2)_3(fma)_6]\cdot 6fma$ with Ln/X = La/Cl(1), La/Br(2), Eu/Cl(3), and Eu/Br(4)

Compounds **1–4** are isostructural and, therefore, only the structure of compound **3** will be described in detail with a comparative study for the other compounds. Compounds **1–4** crystallize in the triclinic *P*-1 space group. The asymmetric unit (Figure 1a) contains one Ln^{III} ion, three half anilato ligands, three coordinated fma molecules, and three crystallization fma molecules. The general formula is, then, $[Ln_2(C_6O_4X_2)_3(fma)_6]\cdot 6fma$ with Ln/X = La/Cl (**1**), La/Br (**2**), Eu/Cl (**3**), and Eu/Br (**4**).

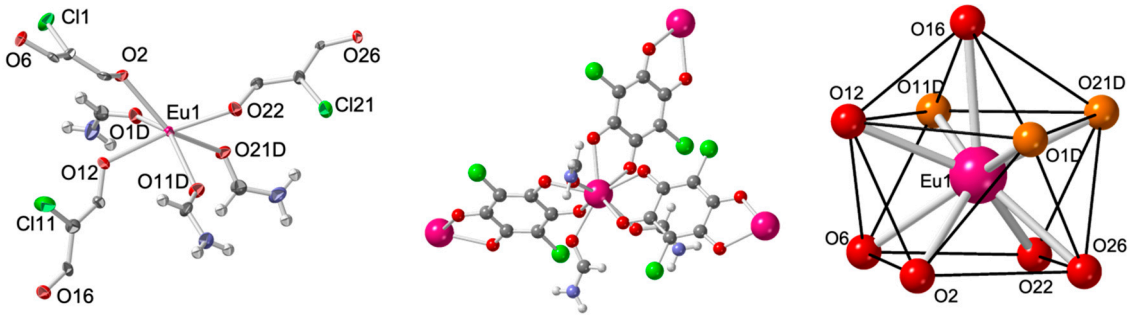

(**a**) (**b**) (**c**)

Figure 1. (**a**) ORTEP plot of the asymmetric unit of compound **3** showing the labelling scheme. Crystallization fma molecules are omitted for clarity. Ellipsoids are drawn at 80% probability. (**b**) Coordination environment around the Eu centre in compound **3**. Colour code: Eu = pink, C = grey, O = red, N = blue, Cl = green, and H = white. (**c**) Caped square antiprism coordination geometry around the Eu ion in compound **3**. The O atoms of the fma molecules are drawn in orange.

Each metal centre is coordinated by three chelating anilato ligands and completes its nona-coordination with three fma molecules. These three anilato ligands connect each Ln^{III} with three other metal centres (Figure 1b). The Ln^{III} ion is surrounded by nine O atoms: O2, O6, O12, O16, O22, and O26, from the three chelating anilato ligands, and O1D, O11D, and O21D, from the three coordinated fma molecules (Figure 1c). Continuous SHAPE analysis of the coordination environment shows that the coordination geometry of the metal centres is a slightly distorted caped square antiprism (CSAPR-9, Table 3) [39].

Table 3. Continuous SHAPE measurement (CShM) values of the 13 possible coordination geometries for the Ln^{III} ion with coordination number nine in compounds **1**–**4**. The minimum values are indicated in bold.

Geometry	Symmetry	1 (La/Cl)	2 (La/Br)	3 (Eu/Cl)	4 (Eu/Br)
EP-9	D9h	35.526	35.419	35.988	35.960
OPY-9	C8v	22.645	22.742	22.286	22.320
HBPY-9	D7h	19.617	19.309	19.753	19.516
JTC-9	C3v	14.629	14.642	15.021	14.981
JCCU-9	C4v	10.075	9.946	9.914	9.827
CCU-9	C4v	8.982	8.864	8.932	8.842
JCSAPR-9	C4v	1.389	1.383	1.120	1.146
CSAPR-9	**C4v**	**0.478**	**0.487**	**0.318**	**0.348**
JTCTPR-9	D3h	2.866	2.986	2.644	2.825
TCTPR-9	D3h	1.592	1.618	1.369	1.490
JTDIC-9	C3v	12.091	12.151	12.273	12.234
HH-9	C2v	11.162	11.111	11.641	11.504
MFF-9	Cs	0.969	0.975	0.882	0.870

EP-9 = Enneagon; OPY-9 = Octagonal pyramid; HBPY-9 = Heptagonal bipyramid; JTC-9 = Triangular cupola (J3 = trivacant cuboctahedron); JCCU-9 = Capped cube (Elongated square pyramid, J8); CCU-9 = Capped cube; JCSAPR-9 = Capped square antiprism (Gyroelongated square pyramid J10); **CSAPR-9 = Capped square antiprism**; JTCTPR-9 = Tricapped trigonal prism (J51); TCTPR-9 = Tricapped trigonal prism; JTDIC-9 = Tridiminished icosahedron (J63); HH-9 = Hula hoop; MFF-9 = Muffin.

A close look at the coordination environment of the Ln^{III} ions (Figure 1c) shows that the fma O atoms occupy the upper square face of the CSAPR. We call this a *030* location, (where the two first digits refer to the number of solvent molecules in the lower and upper square faces, respectively, and the third one to the capping position). As we will see below, the exact position of the O atoms of the fma molecules and of the anilato ligands determines the spatial orientation of the bridging anilato ligands and, thus, the distortions of the hexagonal cavities and the final structure.

The connectivity of the metal ions through the anilato ligands gives rise to a two-dimensional structure with a (6,3)-gon topology where each metal atom is connected to three other metal atoms, forming very distorted, almost rectangular, six-membered rings, disposed in flat layers and formulated as $[Ln_2(C_6O_4X_2)_3(fma)_6]$ (Figure 2). The crystallization fma molecules are located in between these layers as well as inside the layers in the cavities. The coordinated fma molecules are located orthogonal to the layers, pointing towards the interlayer space (Figure 2).

The cavities are arranged in parallel to their long axis with a brick wall disposition (Figure 3a). In each cavity, four of the anilato ligands are disposed perpendicular (*edge on*) and two perpendicular (*face on*) to the cavity plane (Figure 3a). The layers are packed parallel to the *bc* plane in an eclipsed way, giving rise to channels running along the *a* direction (Figure 3b).

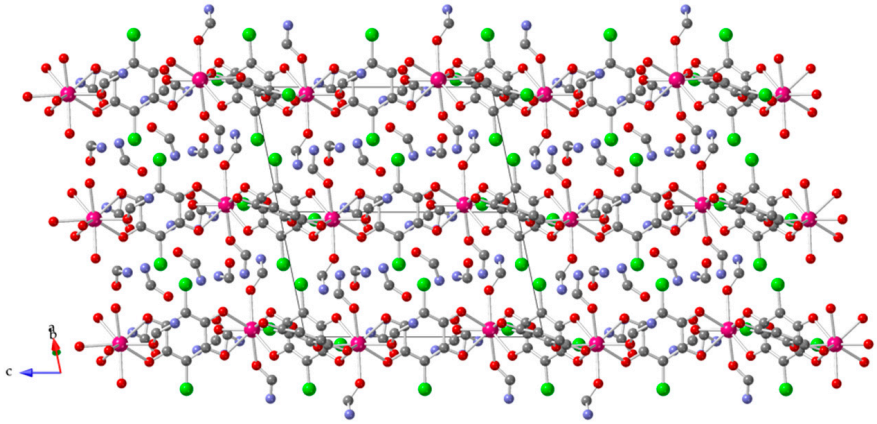

Figure 2. View of three consecutive layers in compound **3** showing the coordinated fma molecules pointing towards the interlayer space and the crystallization fma molecules located in between the layers. Colour code: Eu = pink, C = grey, O = red, N = blue, Cl = green, and H = white.

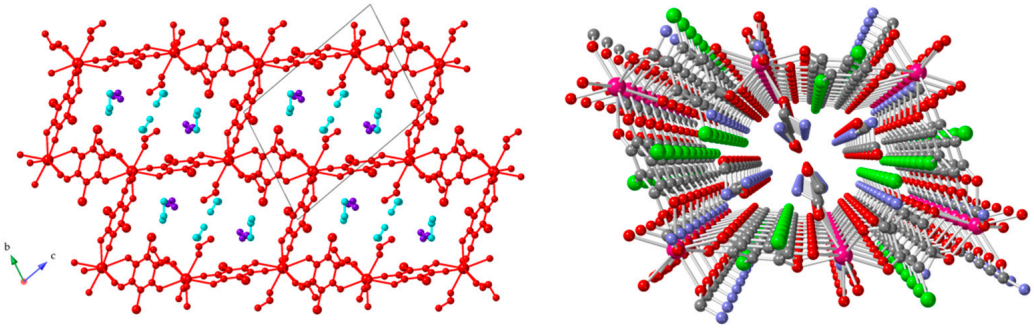

(**a**) (**b**)

Figure 3. (**a**) View, down the *a* direction, of one brick wall-like layer parallel to the *bc* plane in compound **3** showing the crystallization fma molecules located above and below (light blue), and inside (purple) the layers. (**b**) Perspective view of one rectangular channel along the *a* direction in compound **3** showing the fma molecules inside the channels. Colour code in (**b**): Eu = pink, C = grey, O = red, N = blue, Cl = green, and H = white.

4. Discussion

The structure of compounds **1**–**4** is similar to the *c*-type structure reported by Robson et al. [23,25], with water as coordinated solvent, and has the same (6,3)-gon topology found in other Ln-containing anilato-based lattices [22].

If we compare in detail the structures of compounds **1**–**4**, we can observe that the average Ln-O_{fma} bond distances are shorter than the Ln-$O_{anilato}$ ones in all cases (Table 4). This difference can be attributed to the rigidity of the five-membered chelate rings formed with the anilato ligands. As expected, the La-O bond distances (**1** and **2**) are longer than the Eu-O ones (**3** and **4**), since La^{III} is larger than Eu^{III}. If we compare the two compounds with the same Ln^{III} ion, we can see that the Ln-$O_{anilato}$ bond distances for the chloranilato compounds are slightly shorter than the corresponding ones with bromanilato. Although the difference is small, this difference has to be attributed to the larger steric hindrance of the Br atoms, since the electronic effects should lead to the opposite trend (the O atoms of chloranilato have less electron density and, therefore, should form longer Ln-O bonds).

Table 4. Ln-O bond distances (in Å) in compounds **1**–**4**.

Atoms	1 (La/Cl)	2 (La/Br)	3 (Eu/Cl)	4 (Eu/Br)
Ln-O2	2.557(4)	2.622(5)	2.454(3)	2.453(5)
Ln-O6	2.614(4)	2.566(4)	2.465(3)	2.453(5)
Ln-O12	2.548(4)	2.556(5)	2.455(3)	2.465(5)
Ln-O16	2.552(4)	2.557(5)	2.548(3)	2.548(5)
Ln-O22	2.526(4)	2.544(4)	2.444(3)	2.477(5)
Ln-O26	2.544(4)	2.539(4)	2.459(3)	2.483(5)
Ln-O1D	2.503(4)	2.520(4)	2.377(3)	2.382(5)
Ln-O11D	2.468(4)	2.508(5)	2.418(3)	2.413(5)
Ln-O21D	2.508(4)	2.483(4)	2.400(3)	2.429(5)
Ln-$O_{anilato}$ [1]	2.557	2.564	2.471	2.480
Ln-O_{fma} [2]	2.493	2.504	2.398	2.408

[1] Average Ln-O bond distance of the anilato oxygen atoms: O2, O6, O12, O16, O22, and O26 (O6, O16, and O26 correspond to O3, O13, and O23, respectively, in compound **2**). [2] Average Ln-O bond distance of the fma oxygen atoms.

The distortions of the hexagonal cavities in **3** can be quantified by the three Ln-Ln distances along the diagonals of the distorted hexagonal cavity (20.74, 17.78, and 11.36 Å), as well as by the three Ln-Ln-Ln angles (87.30, 109.02, and 159.18°). These values in the other compounds are similar, although, as expected, the Ln-Ln distances are longer in the La^{III} compounds (**1** and **2**) than in the Eu^{III} ones (**3** and **4**, Table 5). On the other side, if we compare the chloranilato and bromanilato derivatives for the same lanthanoid, we can see that in the bromanilato derivatives (**2** and **4**), the Ln-Ln distances are slightly longer than in the corresponding chloranilato ones (**1** and **3**), as a consequence of the larger steric hindrance of Br. In contrast, the Ln-Ln-Ln angles do not show a general trend since they are correlated and the decrease of one of them leads to an increase of the others.

Table 5. Ln-Ln diagonal distances (in Å) and Ln-Ln-Ln angles (in °) in compounds **1**–**4**.

	1 (La/Cl)	2 (La/Br)	3 (Eu/Cl)	4 (Eu/Br)
Ln-Ln (Å)	21.27	21.30	20.74	20.85
	18.07	18.15	17.78	17.83
	11.43	11.54	11.36	11.47
Ln-Ln-Ln (°)	86.11	86.61	87.30	87.37
	109.05	109.15	109.02	109.48
	159.92	159.71	159.18	159.07

As can be observed in Table 3, although the coordination geometry of the Ln^{III} ions is caped square antiprism (CSAPR-9) in all cases, the two compounds with La^{III} show higher SHAPE parameter values (0.478 in **1** and 0.487 in **2**) than the Eu^{III} derivatives (0.318 in **3** and 0.348 in 4). The larger distortions in the La^{III} derivatives are due to the larger size of La^{III} compared to Eu^{III} and has already been observed in other anilato-based compounds with other solvent molecules [26]. Furthermore, for both lanthanoids, the compounds with bromanilato (**2** and **4**) show larger distortions from the ideal geometry than the corresponding chloranilato ones (**1** and **3**). This fact reflects the larger steric hindrance of the Br atoms in bromanilato compared to Cl in chloranilato.

Although La^{III} and Eu^{III} have different sizes, they present the same coordination number (nine) and geometry (CSAPR-9). This fact can be explained by the small size and steric hindrance of the fma molecule that allows the coordination of three molecules, even for the smaller Eu^{III} ion. Note also that although the larger size of La^{III} might lead to a coordination number of ten, this high coordination number has only been observed once with anilato ligands and La^{III}, and in that case, the additional ligand was H_2O [22,25].

5. Conclusions

We have synthesized and structurally characterized four isostructural anilato-based compounds with La^{III} and Eu^{III} and formamide as solvent. These compounds, formulated as $[Ln_2(C_6O_4X_2)_3(fma)_6]\cdot 6fma$ with Ln/X = La/Cl (**1**), La/Br (**2**), Eu/Cl (**3**), and Eu/Br (**4**), with $C_6O_4X_2^{2-}$ = chloranilato (X = Cl) and bromanilato (X = Br), crystallize in the triclinic *P*-1 space group. The Ln^{III} centres are surrounded by nine oxygen atoms from three chelating anilato ligands and three coordinated formamide molecules. The coordination geometry is slightly distorted caped square antiprism with a *030* disposition of the three fma solvent molecules. The spatial orientation of the anilato ligands around the metal ions leads to a two-dimensional structure with a (6,3)-gon topology with very distorted hexagonal cavities that appear as rectangles showing a brick wall disposition in the layers. There are formamide crystallization molecules located in between the layers and in the rectangular channel formed by the eclipsed packing of the layers.

A detailed comparative analysis in compounds **1**–**4** of the influence of the size of the lanthanoid and of the X group of the anilato ligand in the structural parameters, shows that: (i) the La^{III} compounds present a higher distortion of the coordination geometry than the Eu^{III} ones, (ii) the bromanilato compounds present a higher distortion than the corresponding chloranilato ones, (iii) the Ln^{III}-O bond distances are larger for the La^{III} compounds than for the Eu^{III} ones, (iv) the Ln^{III}-O bond distances are larger for the bromanilato derivatives than for the chloranilato ones, and (v) the distortions of the rectangular cavities are larger for the La^{III} compounds and for the bromanilato derivatives. All these differences can be explained by the larger size of La^{III} compared to Eu^{III} and by the larger steric hindrance of Br.

The results reported here open the gate to the synthesis of the corresponding compounds with other lanthanoids to confirm the influence of the lanthanoid size and to check for possible changes in the coordination number and in the structure as the Ln^{III} size decreases. On the other hand, an optical study is ongoing for the four compounds. We are also preparing the Dy^{III} and Er^{III} derivatives with both anilato ligands in order to obtain single-ion magnet behaviour, as has already been observed in other anilato-based Dy^{III} and Er^{III} compounds with different solvents [22]. Work is in progress.

Supplementary Materials: The following supporting information can be downloaded at: https://www.mdpi.com/article/10.3390/cryst13060939/s1, Tables S1–S4: main bond distances (in Å) in compounds **1**–**4**, respectively. Table S5. Main IR bands and their assignments in compounds **1**–**4**. Figures S1–S4: IR spectra of compounds **1**–**4**, respectively.

Author Contributions: Conceptualization, S.B. and C.J.G.-G.; data curation, S.B., C.J.G.-G., A.H.-P. and K.D.-A.; formal analysis, S.B. and C.J.G.-G.; funding acquisition, C.J.G.-G.; investigation, S.B., C.J.G.-G. and A.H.-P.; methodology, S.B., C.J.G.-G., A.H.-P. and K.D.-A.; project administration, C.J.G.-G.; supervision, S.B. and C.J.G.-G.; writing—original draft, C.J.G.-G.; writing—review and editing, S.B., C.J.G.-G. and A.H.-P. All authors have read and agreed to the published version of the manuscript.

Funding: This study forms part of the Advanced Materials program and was supported by the Spanish MCIN with funding from European Union NextGeneration EU (PRTR- C17.I1) and the Generalitat Valenciana (project MFA-2022-057). We also thank the project PID2021-125907NB-I00, financed by MCIN/AEI/10.13039/50110 0 011033/FEDER, UE, for financial support.

Data Availability Statement: The data presented in this study are available on request from the corresponding author.

Conflicts of Interest: The authors declare no conflict of interest. The funders had no role in the design of the study; in the collection, analyses, or interpretation of data; in the writing of the manuscript, or in the decision to publish the results.

References

1. Batten, S.R.; Champness, N.R.; Chen, X.; Garcia-Martinez, J.; Kitagawa, S.; Öhrström, L.; O'Keeffe, M.; Suh, M.P.; Reedijk, J. Terminology of metal–organic Frameworks and Coordination Polymers (IUPAC Recommendations 2013). *Pure Appl. Chem.* **2013**, *85*, 1715–1724. [CrossRef]
2. Zhang, X.; Chen, Z.; Liu, X.; Hanna, S.L.; Wang, X.; Taheri-Ledari, R.; Maleki, A.; Li, P.; Farha, O.K. A Historical Overview of the Activation and Porosity of metal–organic Frameworks. *Chem. Soc. Rev.* **2020**, *49*, 7406–7427. [CrossRef]
3. Zhou, H.C.; Long, J.R.; Yaghi, O.M. Introduction to Metal-Organic Frameworks. *Chem. Rev.* **2012**, *112*, 673–674. [CrossRef]
4. Furukawa, H.; Cordova, K.E.; O'Keeffe, M.; Yaghi, O.M. The Chemistry and Applications of Metal-Organic Frameworks. *Science* **2013**, *341*, 1230444. [CrossRef]
5. Zhao, X.; Wang, Y.; Li, D.; Bu, X.; Feng, P. Metal–Organic Frameworks for Separation. *Adv. Mater.* **2018**, *30*, 1705189. [CrossRef] [PubMed]
6. Shu-Na, Z.; Wang, G.; Poelman, D.; Van Der Voort, P. Metal Organic Frameworks Based Materials for Heterogeneous Photocatalysis. *Molecules* **2018**, *23*, 2947.
7. Li, H.; Zhao, S.; Zang, S.; Li, J. Functional metal–organic Frameworks as Effective Sensors of Gases and Volatile Compounds. *Chem. Soc. Rev.* **2020**, *49*, 6364–6401. [CrossRef] [PubMed]
8. Kreno, L.E.; Leong, K.; Farha, O.K.; Allendorf, M.; Van Duyne, R.P.; Hupp, J.T. Metal-Organic Framework Materials as Chemical Sensors. *Chem. Rev.* **2012**, *112*, 1105–1125. [CrossRef]
9. Campbell, M.G.; Dinca, M. Metal-Organic Frameworks as Active Materials in Electronic Sensor Devices. *Sensors* **2017**, *17*, 1108. [CrossRef]
10. Canivet, J.; Fateeva, A.; Guo, Y.; Coasne, B.; Farrusseng, D. Water Adsorption in MOFs: Fundamentals and Applications. *Chem. Soc. Rev.* **2014**, *43*, 5594–5617. [CrossRef]
11. Marin, R.; Brunet, G.; Murugesu, M. Shining New Light on Multifunctional Lanthanide Single-Molecule Magnets. *Angew. Chem. Int. Ed.* **2021**, *60*, 1728–1746. [CrossRef] [PubMed]
12. Rocha, J.; Carlos, L.D.; Paz, F.A.A.; Ananias, D. Luminescent Multifunctional Lanthanides-Based metal–organic Frameworks. *Chem. Soc. Rev.* **2011**, *40*, 926–940. [CrossRef] [PubMed]
13. Chakraborty, G.; Park, I.; Medishetty, R.; Vittal, J.J. Two-Dimensional Metal-Organic Framework Materials: Synthesis, Structures, Properties and Applications. *Chem. Rev.* **2021**, *121*, 3751–3891. [CrossRef] [PubMed]
14. Wang, M.; Dong, R.; Feng, X. Two-Dimensional Conjugated metal–organic Frameworks (2D c-MOFs): Chemistry and Function for MOFtronics. *Chem. Soc. Rev.* **2021**, *50*, 2764–2793. [CrossRef]
15. Benmansour, S.; Vallés-García, C.; Gómez-Claramunt, P.; Mínguez Espallargas, G.; Gómez-García, C.J. 2D and 3D Anilato-Based Heterometallic M(I)M(III) Lattices: The Missing Link. *Inorg. Chem.* **2015**, *54*, 5410–5418. [CrossRef]
16. Atzori, M.; Artizzu, F.; Sessini, E.; Marchio, L.; Loche, D.; Serpe, A.; Deplano, P.; Concas, G.; Pop, F.; Avarvari, N.; et al. Halogen-Bonding in a New Family of Tris(Haloanilato)Metallate(III) Magnetic Molecular Building Blocks. *Dalton Trans.* **2014**, *43*, 7006–7019. [CrossRef]
17. Benmansour, S.; Gómez-Claramunt, P.; Vallés-García, C.; Mínguez Espallargas, G.; Gómez García, C.J. Key Role of the Cation in the Crystallization of Chiral Tris(Anilato)Metalate Magnetic Anions. *Cryst. Growth Des.* **2016**, *16*, 518–526. [CrossRef]
18. Kitagawa, S.; Kawata, S. Coordination Compounds of 1,4-Dihydroxybenzoquinone and its Homologues. Structures and Properties. *Coord. Chem. Rev.* **2002**, *224*, 11–34. [CrossRef]
19. Abrahams, B.F.; Grannas, M.J.; Hudson, T.A.; Hughes, S.A.; Pranoto, N.H.; Robson, R. Synthesis, Structure and Host-Guest Properties of $(Et_4N)_2[Sn^{IV}Ca^{II}(Chloranilate)_4]$, a New Type of Robust Microporous Coordination Polymer with a 2D Square Grid Structure. *Dalton Trans.* **2011**, *40*, 12242–12247. [CrossRef]
20. Benmansour, S.; Gómez-García, C.J. A Heterobimetallic Anionic 3,6-Connected 2D Coordination Polymer Based on Nitranilate as Ligand. *Polymers* **2016**, *8*, 89. [CrossRef]
21. Mercuri, M.L.; Congiu, F.; Concas, G.; Sahadevan, S.A. Recent Advances on Anilato-Based Molecular Materials with Magnetic and/or Conducting Properties. *Magnetochemistry* **2017**, *3*, 17. [CrossRef]
22. Benmansour, S.; Gómez-García, C.J. Lanthanoid-Anilato Complexes and Lattices. *Magnetochemistry* **2020**, *6*, 71. [CrossRef]
23. Riley, P.E.; Haddad, S.F.; Raymond, K.N. Preparation of Praseodymium(III) Chloranilate and the Crystal Structures of $Pr_2(C_6Cl_2O_4)_3 \cdot 8C_2H_5OH$ and $Na_3[C_6H_2O(OH)(SO_3)_2] \cdot H_2O$. *Inorg. Chem.* **1983**, *22*, 3090–3096. [CrossRef]
24. Abrahams, B.F.; Coleiro, J.; Hoskins, B.F.; Robson, R. Gas Hydrate-like Pentagonal Dodecahedral $M_2(H_2O)_{18}$ cages (M = Lanthanide or Y) in 2,5-Dihydroxybenzoquinone-Derived Coordination Polymers. *Chem. Commun.* **1996**, *5*, 603–604. [CrossRef]
25. Abrahams, B.F.; Coleiro, J.; Ha, K.; Hoskins, B.F.; Orchard, S.D.; Robson, R. Dihydroxybenzoquinone and Chloranilic Acid Derivatives of Rare Earth Metals. *J. Chem. Soc. Dalton Trans.* **2002**, *8*, 1586–1594. [CrossRef]
26. Benmansour, S.; Gómez-García, C.J.; Hernández-Paredes, A. The Complete Series of Lanthanoid-Chloranilato Lattices with Dimethylsulfoxide: Role of the Lanthanoid Size on the Coordination Number and Crystal Structure. *Crystals* **2022**, *12*, 261. [CrossRef]
27. Benmansour, S.; Hernández-Paredes, A.; Gómez-García, C.J. Effect of the Lanthanoid-Size on the Structure of a Series of Lanthanoid-Anilato 2-D Lattices. *J. Coord. Chem.* **2018**, *71*, 845–863. [CrossRef]

28. Gómez-Claramunt, P.; Benmansour, S.; Hernández-Paredes, A.; Cerezo-Navarrete, C.; Rodríguez-Fernández, C.; Canet-Ferrer, J.; Cantarero, A.; Gómez-García, C.J. Tuning the Structure and Properties of Lanthanoid Coordination Polymers with an Asymmetric Anilato Ligand. *Magnetochemistry* **2018**, *4*, 6. [CrossRef]
29. Benmansour, S.; Hernández-Paredes, A.; Gómez-García, C.J. Two-Dimensional Magnetic Coordination Polymers Formed by Lanthanoids and Chlorocyananilato. *Magnetochemistry* **2018**, *4*, 58. [CrossRef]
30. Kharitonov, A.D.; Trofimova, O.Y.; Meshcheryakova, I.N.; Fukin, G.K.; Khrizanforov, M.N.; Budnikova, Y.H.; Bogomyakov, A.S.; Aysin, R.R.; Kovalenko, K.A.; Piskunov, A.V. 2D-metal–organic Coordination Polymers of Lanthanides (La(III), Pr(III) and Nd(III)) with Redox-Active Dioxolene Bridging Ligands. *CrystEngComm* **2020**, *22*, 4675–4679. [CrossRef]
31. Benmansour, S.; Pintado-Zaldo, C.; Martínez-Ponce, J.; Hernández-Paredes, A.; Valero-Martínez, A.; Gómez-Benmansour, M.; Gómez-García, C.J. The Versatility of Ethylene Glycol to Tune the Dimensionality and Magnetic Properties in DyIII-Anilato-Based Single-Ion Magnets. *Cryst. Growth Des.* **2023**, *23*, 1269–1280. [CrossRef]
32. Benmansour, S.; Pérez-Herráez, I.; Cerezo-Navarrete, C.; López-Martínez, G.; Martínez Hernandez, C.; Gómez-García, C.J. Solvent-Modulation of the Structure and Dimensionality in Lanthanoid-Anilato Coordination Polymers. *Dalton Trans.* **2018**, *47*, 6729–6741. [CrossRef] [PubMed]
33. Benmansour, S.; Hernández-Paredes, A.; Mondal, A.; López Martínez, G.; Canet-Ferrer, J.; Konar, S.; Gómez-García, C.J. Slow Relaxation of the Magnetization, Reversible Solvent Exchange and Luminescence in 2D Anilato-Based Frameworks. *Chem. Commun.* **2020**, *56*, 9862–9865. [CrossRef] [PubMed]
34. Oxford Diffraction CrysalisPro. 2004. 171.33.55. Available online: https://www.rigaku.com/products/crystallography/crysalis (accessed on 27 April 2023).
35. Altomare, A.; Burla, M.C.; Camalli, M.; Cascarano, G.L.; Giacovazzo, C.; Guagliardi, A.; Moliterni, A.G.G.; Polidori, G.; Spagna, R. SIR97: A New Tool for Crystal Structure Determination and Refinement. *J. Appl. Cryst.* **1999**, *32*, 115–119. [CrossRef]
36. Sheldrick, G.M. Crystal Structure Refinement with SHELXL. *Acta Cryst. C* **2015**, *71*, 3–8. [CrossRef]
37. Farrugia, L.J. WinGX and ORTEP for Windows: An Update. *J. Appl. Cryst.* **2012**, *45*, 849–854. [CrossRef]
38. Álvarez, S. Coordinating Ability of Anions, Solvents, Amino Acids, and Gases Towards Alkaline and Alkaline-Earth Elements, Transition Metals, and Lanthanides. *Chem. Eur. J.* **2020**, *26*, 4350–4377. [CrossRef]
39. Álvarez, S. Distortion Pathways of Transition Metal Coordination Polyhedra Induced by Chelating Topology. *Chem. Rev.* **2015**, *115*, 13447–13483. [CrossRef]